Physica Scripta

PAPER

Collisions of highly charged ions with hydrogen relevant to plasma diagnostics

To cite this article: Clara Illescas *et al* 2013 *Phys. Scr.* **2013** 014033

Phys. Scr. **T156** (2013) 014033 (4pp) doi:10.1088/0031-8949/2013/T156/014033

Collisions of highly charged ions with hydrogen relevant to plasma diagnostics

Clara Illescas, L F Errea and L Méndez

Laboratorio Asociado al CIEMAT de Física Atómica y Molecular en Plasmas de Fusión, Departamento de Química, Universidad Autónoma de Madrid, E-28049 Madrid, Spain

E-mail: clara.illescas@uam.es

Received 3 September 2012
Accepted for publication 21 November 2012
Published 23 September 2013
Online at stacks.iop.org/PhysScr/T156/014033

Abstract
We present total cross sections for ionization, and total and nl-partial cross sections for electron capture in collisions of Kr^{36+} and W^{60+} with H(1s). Calculations have been carried out using the classical trajectory Monte Carlo method. We have found that scaling laws as functions of the ion charge are valid for total electron capture cross sections, but they are less accurate for n-partial cross sections. The nl-partial cross sections show l distributions similar to those found for collisions with Ar^{18+} by Errea *et al* (2006 *J. Phys. B: At. Mol. Opt. Phys.* **39** L91).

PACS numbers: 34.10.+x, 34.70.+e

(Some figures may appear in color only in the online journal)

1. Introduction

Charge exchange recombination spectroscopy (CXRS) [1] is a powerful diagnostic tool commonly used in tokamak devices and will be employed as the main diagnostic of ITER [2]. In practice, an energetic beam of atoms, usually hydrogen, deuterium or helium, is injected into the reactor. Collisions of these atoms with the core plasma ions lead to the formation of highly excited species, whose emission is employed to determine the temperature and density of the plasma. Noble gases are often puffed into the divertor region to improve plasma confinement conditions [3], and the noble gas atoms become fully ionized in the core region. Specifically, addition of krypton yields Kr^{+36} ions, which give rise to the electron capture (EC), also called charge exchange, reaction with neutral beam atoms. For the particular case of a hydrogen (deuterium) beam, the process

$$Kr^{36+} + H(D) \rightarrow Kr^{35+}(nl) + H(D)^{+} \qquad (1)$$

takes place, and the CXRS diagnostic is based on the ensuing emission by Kr^{35+}.

The CXRS diagnostic is also applied to determine the density of impurity ions formed initially by sputtering of plasma facing components. In this respect, tungsten ions are one of the most relevant impurities, and in this case partially stripped species are expected to be present in the core plasma. It is important to note the lack of data for EC with these highly charged species, which are also of great importance in determining the ionization balance of EBIT plasmas [4]. K-shell x-ray emission measurements [5] and recent calculations have been reported for argon and tungsten (with charge $Z \leqslant 40$) ions, respectively [6]. In this work, we have studied collisions with W^{60+}. Generally, CXRS employs frequencies in the visible spectrum. For the systems considered in this work, the transitions $n \rightarrow n-1$ of interest are those with $n = 22$–28 for Kr^{35+} and $n = 30$–40 for W^{59+}.

It is important to note that CXRS diagnostics require accurate cross sections for population of very excited energy levels of the ion formed in the EC process; this precludes the use of close-coupling methods that would involve prohibitively large expansions. Besides, at the energies of neutral beams ($E > 40\,\mathrm{keV\,amu^{-1}}$), ionization cross sections are of the same order of magnitude or larger than the EC ones, requiring a simultaneous description of both processes. At these collision energies, the classical trajectory Monte Carlo (CTMC) method [7] is the preferred method to evaluate ionization and both total and state selective EC cross sections. In this work, we have applied the eikonal-CTMC method previously used for $B^{5+} + H$ [8, 9], $Ne^{10+} + H$ [10] and $Ar^{16+,17+,18+} + H$ [11] collisions.

The aim of this work is to check the possibility of applying Z-scaling laws for total and partial EC cross

sections, which could avoid explicit calculations for population of highly excited levels. In particular, scaling laws have been proposed in [12] and are implemented in the ADAS database [13].

Atomic units ($\hbar = 1$, $e = 1$, $m_e = 1$) are used unless otherwise stated.

2. Computational method

In the eikonal-CTMC treatment (see [14]), the projectile follows straight-line trajectories with impact parameter b and velocity v and the electron motion is described by means of a classical distribution function $\rho(\boldsymbol{r}, \boldsymbol{p}, t)$. The distribution is discretized in a set of N independent electron trajectories, obtained by integrating the corresponding Hamilton equations. For a one-electron system, the Hamiltonian has the form

$$H(\boldsymbol{r}, \boldsymbol{p}, t) = \frac{p^2}{2} - \frac{1}{r_H} + V_p(r_p), \tag{2}$$

where r_H and r_p are, respectively, the electron distances to the hydrogen and the projectile nuclei. In our calculation, $V_p(r_p) = -Z/r_p$, with $Z = 36$ for Kr^{36+} and $Z = 60$ for W^{60+}, i.e. we treat this second system as a fully stripped ion (Nd^{60+}). This approach is expected to be valid for population of highly excited states such as those relevant to CXRS. In our calculation, ρ is initially a superposition of ten microcanonical distributions with different energies E_k that fit the quantal radial distribution of the hydrogen 1s orbital [15]:

$$\rho(\boldsymbol{r}, \boldsymbol{p}, -\infty) = \sum_{k=1}^{10} a_k \delta(H - E_k). \tag{3}$$

In practice, we have considered $N = 3 \times 10^5$ trajectories that have been integrated up to a final time $t_f = 1500$ au. At the end of the collision the distribution is analyzed to evaluate EC $P^{EC}(b, v)$ and ionization probabilities $P^I(b, v)$:

$$P^{EC}(b, v) = \frac{N^{EC}}{N}, \quad P^I(b, v) = \frac{N^I}{N}, \tag{4}$$

where N^{EC} is the number of trajectories in which the electron is bound to the ion nucleus at $t \to \infty$ and N^I is the number of trajectories where the electron is unbound. In order to evaluate EC partial cross sections, we divide the phase space in boxes associated to each quantum state [16]. Specifically,

$$\begin{aligned} &n(n-1/2)(n-1) < n_c^3 \leqslant n(n+1/2)(n+1), \\ &l < \frac{n}{n_c} l_c \leqslant l+1, \end{aligned} \tag{5}$$

where $n_c = Z/\sqrt{2E_p}$. E_p and l_c are, respectively, the electron energy and angular momentum in the projectile reference frame. The probability of populating a given quantal state is then given by the fraction of trajectories that arrive at the corresponding box after the collision:

$$P_{nl}^{EC}(b, v) = \frac{N_{nl}^{EC}}{N} \tag{6}$$

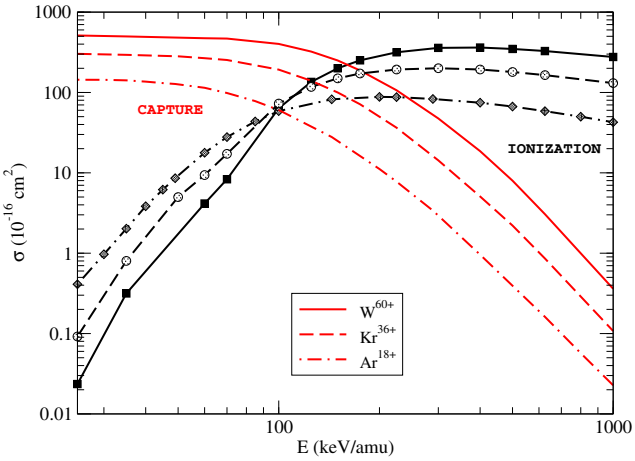

Figure 1. Total cross sections for EC and ionization for Ar^{18+}, Kr^{36+} and W^{60+} collisions with H(1s).

and the nl-partial EC cross sections and total cross sections are then obtained as

$$\begin{aligned} &\sigma_{nl}^{EC}(v) = 2\pi \int_0^\infty b P_{nl}^{EC}(b, v)\, db, \quad \sigma_n^{EC}(v) = \sum_{l=0}^{n-1} \sigma_{nl}^{EC}, \\ &\sigma^{EC,I}(v) = 2\pi \int_0^\infty b P^{EC,I}(b, v)\, db. \end{aligned} \tag{7}$$

3. Results and discussion

In figure 1, we show the total cross sections for ionization and EC for the two collisions considered. To our knowledge, there are no previous experimental or theoretical data for these two systems. For comparison, we have included in the figure the CTMC cross sections of [11] for Ar^{18+} + H(1s). It can be noted that, while the EC cross section increases with Z, at $E < 100$ keV amu^{-1} the ionization cross section decreases when Z increases. At these relatively low energies, the ionization and capture mechanisms involve initially the polarization of the electronic cloud, which is then either captured by the projectile or ionized, with a larger capture probability for systems with larger Z, and accordingly a smaller ionization probability. However, at high impact energies, direct ionization is the dominant process, which takes place through projectile–electron inelastic collisions that yield larger ionization probabilities for larger Z. The different ionization mechanism explains the re-ordering of the ionization cross sections for the three systems of figure 1 at $E \approx 100$ keV amu^{-1}.

In order to check the workings of the scaling law derived in [12] by fitting available EC cross sections for $Z \leqslant 18$, we have plotted in figure 2 our scaled total EC cross section $\sigma^* = \sigma Z^{-\alpha}$ as a function of the scaled energy $E^* = E Z^{-\beta}$, with $\alpha = 1.05$ and $\beta = 0.30$ [12]. The good agreement of our results with the prediction of the scaling law can be noted, which would allow us to predict total EC cross sections for collisions with high Z without performing detailed calculations.

Foster [12] suggests a Z-scaling law for n-partial EC cross sections,

$$\sigma_n^* = \sigma_n Z^{-\delta(E^*)}, \quad n^* = n Z^{-\gamma(E^*)} \tag{8}$$

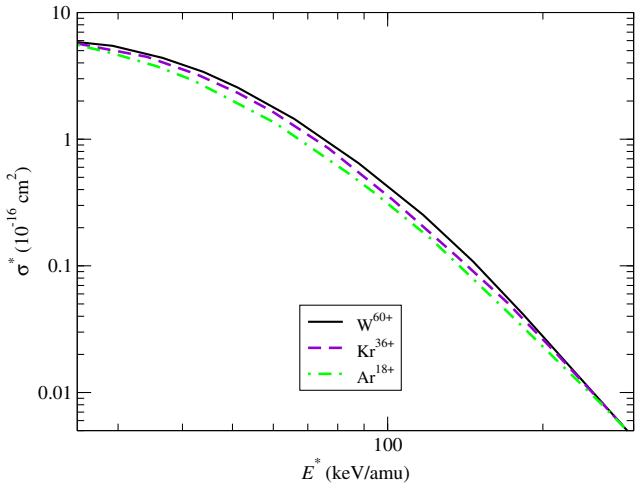

Figure 2. Comparison of the scaled total cross section for EC in Ar^{18+}, Kr^{36+} and W^{60+} collisions with H(1s) as functions of the scaled energy.

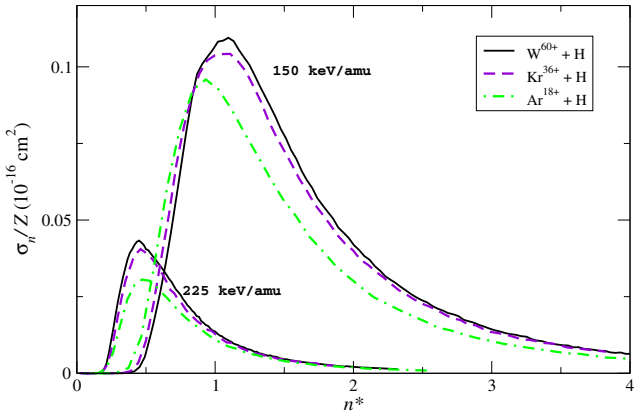

Figure 3. n-partial cross sections for EC in collisions of Ar^{18+}, Kr^{36+} and W^{60+} with H(1s) as functions of the scaled quantum number n^* (see text). The cross sections are divided by the corresponding ion charges, Z.

also based on calculations for $Z \leqslant 18$. As for EC total cross sections, we have checked the validity of (8) for EC from H(1s) by three projectile charges, including the new results for $Z = 36$, 60, and the CTMC cross sections of [11] for $Z = 18$. We plot in figure 3 the calculated σ_n/Z as functions of n^*, for two collision energies. In this figure, we have taken $\gamma = 0.8$ for $E = 150\,\text{keV amu}^{-1}$ and $\gamma = 1.0$ for $E = 225\,\text{keV amu}^{-1}$. The results point out that for highly charged ions the value of δ is very close to one. They also indicate that, at each energy, a single value of γ can be used to fit σ_n/Z for $Z \geqslant 36$. Our calculations at $20 < E < 100\,\text{keV amu}^{-1}$, not shown in the figure, indicate that the scaled n^* correctly predicts the position of the maximum of σ_n^* with $\gamma = 0.8$, but the magnitudes of the cross sections are not accurately fitted. On the other hand, we have checked that, as previously found in other collisions, the n-partial cross sections decay as n^{-3} at high n. This property was explained in [10] as a consequence of the continuity between capture and ionization cross sections.

nl-partial cross sections are shown in figure 4 for two values of n such that $n \to n-1$ transitions lie in the visible spectrum. It can be noted that the l-distributions for both

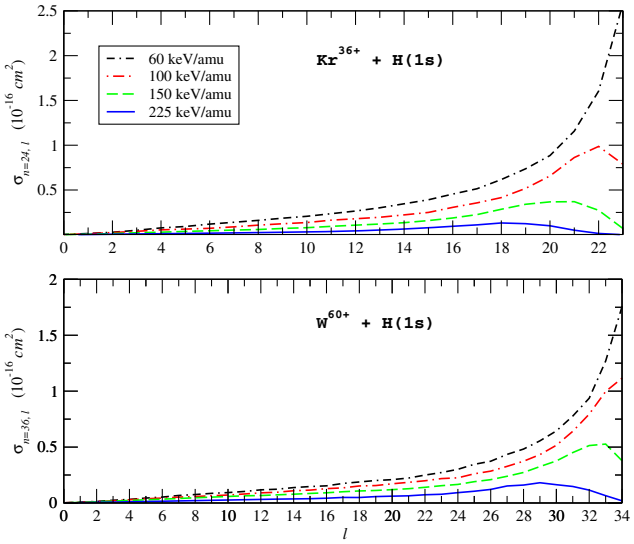

Figure 4. nl-partial cross sections for EC in collisions of H(1s) with Kr^{36+} (top panel) for $n = 24$, and W^{60+} for $n = 36$ (bottom panel), as functions of quantum number l at the four impact energies indicated in the figure.

systems are qualitatively similar and also similar to those reported in [11] for collisions with Ar^{18+}. These results indicate that the shape of these distributions is practically independent of Z. At the lowest energies (illustrated by the results at $60\,\text{keV amu}^{-1}$ in the figure) we find a distribution where $l = n-1$ is the most populated sublevel, as expected from a simple statistical argument, although the calculated cross sections increase exponentially with l. As E increases, the maximum of the distribution moves to lower l, as predicted by perturbative treatments, and, at the highest energies considered in the calculation, the maximum appears at $l \approx Z/2$. At $E < 100\,\text{keV amu}^{-1}$, our results suggest that a simple universal curve

$$\sigma_{nl}^* = \sigma_n \mathcal{F}(l^*; E) \tag{9}$$

with $\sigma_{nl}^* = \sigma_{nl}/\sigma_{nn-1}^*$ and $l^* = l/(n-1)$ can be employed and provides a good approximation at higher energies.

In conclusion, the CTMC method is a useful tool to evaluate the partial EC cross sections required for CXRS diagnostics, which involve both highly charged projectiles and the population of highly excited states. The data generated for the two systems considered in this work support the application of Z-scaling laws to fill the gaps in the existing database.

Acknowledgments

This work has been supported by project numbers ENE2007-62934 and ENE2011-28200 of the Ministerio de Ciencia e Innovación (Spain) and the ADAS-EU Euratom Framework 7 Support Action.

References

[1] Isler R C 1994 *Plasma Phys. Control. Fusion* **36** 171
[2] Marchuk O, Bertschinger G, Biel W, Delabie E, von Hellermann M G, Jaspers R and Reiter D 2008 *Rev. Sci. Instrum.* **79** 10F532

[3] Tokar M Z, Ongena J, Unterberg B and Weinants R R 2000 *Phys. Rev. Lett.* **84** 895
[4] Ralchenko Y, Draganic I N, Tan J N, Gillaspy J D, Pomeroy J M, Reader J, Feldman U and Holland G E 2008 *J. Phys. B: At. Mol. Opt. Phys.* **41** 021003
[5] Allen F I, Biedermann C, Radtke R, Fussmann G and Fritzsche S 2008 *Phys. Rev. A* **78** 032705
[6] Tolstikhina I Y, Song M Y, Imai M, Iriki Y, Itoh A, Kato D, Tawara H, Yoon J S and Shevelko V P 2012 *J. Phys. B: At. Mol. Opt. Phys.* **45** 145201
[7] Abrines R and Percival I C 1966 *Proc. Phys. Soc.* **88** 861
[8] Errea L F, Guzmán F, Illescas C, Méndez L, Pons B, Riera A and Suárez J 2006 *Plasma Phys. Control. Fusion* **48** 1585–604
[9] Guzmán F, Errea L F, Illescas C, Méndez L and Pons B 2010 *J. Phys. B: At. Mol. Opt. Phys.* **43** 144007
[10] Errea L F, Illescas C, Méndez L, Pons B, Riera A and Suárez J 2004 *J. Phys. B: At. Mol. Opt. Phys.* **37** 4323–38
[11] Errea L F, Illescas C, Méndez L, Pons B, Riera A and Suárez J 2006 *J. Phys. B: At. Mol. Opt. Phys.* **39** L91–7
[12] Foster A 2008 *PhD Thesis* University of Strathclyde
[13] Summers H P 2007 *The Atomic Data and Analysis Structure User Manual 2.6* www.adas.ac.uk
[14] Illescas C and Riera A 1999 *Phys. Rev.* A **A60** 4546
[15] Hardie D J W and Olson R E 1983 *J. Phys. B: At. Mol. Phys.* **16** 1983
[16] Becker R L and MacKellar A D 1984 *J. Phys. B: At. Mol. Phys.* **17** 3923